In vivo convergence of BMP and MAPK signaling pathways: impact of differential Smad1 phosphorylation on development and homeostasis

Josée Aubin,[1] Alice Davy, and Philippe Soriano[2]

Program in Developmental Biology, Division of Basic Sciences, Fred Hutchinson Cancer Research Center, Seattle, Washington 98109, USA

Integration of diverse signaling pathways is essential in development and homeostasis for cells to interpret context-dependent cues. BMP and MAPK signaling converge on Smads, resulting in differential phosphorylation. To understand the physiological significance of this observation, we have generated *Smad1* mutant mice carrying mutations that prevent phosphorylation of either the C-terminal motif required for BMP downstream transcriptional activation (*Smad1*^{C} mutation) or of the MAPK motifs in the linker region (*Smad1*^{L} mutation). *Smad1*$^{C/C}$ mutants recapitulate many *Smad1*$^{-/-}$ phenotypes, including defective allantois formation and the lack of primordial germ cells (PGC), but also show phenotypes that are both more severe (head and branchial arches) and less severe (allantois growth) than the null. *Smad1*$^{L/L}$ mutants survive embryogenesis but exhibit defects in gastric epithelial homeostasis correlated with changes in cell contacts, actin cytoskeleton remodeling, and nuclear β-catenin accumulation. In addition, formation of PGCs is impaired in *Smad1*$^{L/L}$ mutants, but restored by allelic complementation in *Smad1*$^{C/L}$ compound mutants. These results underscore the need to tightly balance BMP and MAPK signaling pathways through Smad1.

[*Keywords*: Smad; TGFβ; MAPK; signaling; germ line; homeostasis]

Received March 11, 2004; revised version accepted April 20, 2004.

Cells need to constantly monitor and integrate environmental cues to ensure proper development in the embryo and to maintain tissue homeostasis in the adult. Getting a grasp on how various inputs regulate these processes requires resolving at the cellular level how different signals interact in a concerted fashion to influence cellular processes. TGFβ superfamily members exert a wide range of functions including control of proliferation, migration, terminal differentiation, and cell death (Derynck and Zhang 2003; Siegel and Massagué 2003), processes that are also under the tight influence of sources of MAPK signaling. A puzzling aspect of TGFβ signaling is that despite considerable ligand diversity, signal transduction involves only few receptor combinations and a handful of downstream effectors (or receptor-activated Smads [R-Smads]; Derynck and Zhang 2003). Furthermore, the responses elicited are highly cell-context-dependent, suggesting that other factors or signaling modules influence the outcome. Extracellular and intracellular modulators that modify ligand availability and alter activation at the receptor level may impart specificity in responsiveness (Balemans and Van Hul 2002; Derynck and Zhang 2003).

Another mechanism that may help refine signal outcome is the differential phosphorylation of R-Smads by MAPK signaling (Kretzschmar et al. 1997a, 1999; De Caestecker et al. 1998; Yue et al. 1999; Grimm and Gurdon 2002; Pera et al. 2003; Massagué 2003). MAPK consensus sites are found in all R-Smads, including Smad2 and Smad3 that mediate signaling from TGFβs, Activins and Nodal, and Smad1, Smad5, and Smad8 that relay actions of Bone Morphogenetic Proteins (BMPs), Growth and Differentiation Factors (GDFs), and Anti-Mullerian Hormone (or Mullerian Inhibitory Substance; MIS). This observation suggests that TGFβ and MAPK cross-talk may constitute an important mechanism regulating the cellular outcome of TGFβ signals. TGFβ activates the phosphorylation of serine residues at the C-terminal end of all R-Smads, causing them to form a complex together with the common Smad4 that, in turn, translocates into the nucleus to regulate transcription (Massagué and Wotton 2000). Engagement of receptor tyrosine kinases (RTKs) leads to phosphorylation of MAPK consensus

[1]**Present address: Centre de recherche en cancerologie de l'Université Laval, CHUQ, L'Hôtel-Dieu de Québec, 9 rue McMahon, Québec, QC, Canada G1R 2J6.**
[2]**Corresponding author.**
E-MAIL psoriano@fhcrc.org; FAX (206) 667-6522.
Article and publication are at http://www.genesdev.org/cgi/doi/10.1101/gad.1202604.

sites on R-Smads in the linker region between their conserved Mad Homology 1 (MH1) and MH2 domains (Massagué 2003). In cell culture systems, linker phosphorylation prevents the nuclear localization of the R-Smads, thereby antagonizing TGFβ signaling (Kretzschmar et al. 1997a, 1999). This mechanism has been invoked to explain how oncogenic Ras overrides TGFβ-mediated growth arrest in cancer cells (Kretzschmar et al. 1999). In *Xenopus*, the rapid loss of competence of cells to respond to activin during early embryonic development correlates with phosphorylation of the linker and cytoplasmic retention of Smad2 (Grimm and Gurdon 2002). Similarly, neural induction in *Xenopus* embryos also involves cross-talk between MAPK and TGFβ signaling (Pera et al. 2003). In this case, Fibroblast Growth Factor 8 (FGF8) and Insulin Growth Factor 2 (IGF2) trigger phosphorylation of the Smad1 linker, and together with the sequestrating extracellular molecule Chordin, inhibit BMP-mediated neural induction.

Even though these experimental systems highlight the importance of integrating TGFβ and MAPK signaling, the relevance of this link still needs to be addressed in functional studies that take into account temporal and quantitative requirements. For instance, the extent of R-Smad nuclear exclusion in vitro has been found to be variable (Kretzschmar et al. 1999; Lehmann et al. 2000). Furthermore, the biological significance of modulating the ability of R-Smads to convey TGFβ signaling at physiological levels remains to be determined. To address this issue, we have generated *Smad1* mouse lines that carry mutations at the C-terminal motif required for its transcriptional activity (*Smad1^{C}* mutants), or in the MAPK consensus sites and two conserved phosphoserines of the linker region (*Smad1^{L}* mutants). Because of its extensive biochemical characterization, *Smad1* represents a good model system to decipher the in vivo role of BMP-MAPK regulatory mechanisms (Hoodless et al. 1996; Kretzschmar et al. 1997b; Pera et al. 2003). We show here that, like *Smad1$^{-/-}$* embryos, *Smad1$^{C/C}$* mutants die in utero and display defects in allantois formation and in PGC specification (Lechleider et al. 2001; Tremblay et al. 2001; Hayashi et al. 2002). These observations are consistent with a prominent role for Smad1 in mediating BMP responses. Some phenotypes of the C-terminal mutation are distinct, however, implicating regulation by different signaling pathways. We further show that although the linker mutation does not affect viability, it perturbs PGC formation and stomach homeostasis. At a cellular level, the linker mutation affects cell contacts, actin cytoskeleton, and nuclear β-catenin accumulation, which correlate with retention of Smad1 at the membrane. *Smad1^{C}* and *Smad1^{L}* alleles complement each other in PGC formation, demonstrating that both MAPK and BMP signaling pathways converge on Smad1 to regulate the formation of the germ line. Taken together, these results suggest that MAPK signaling through Smad1 may fulfill other regulatory functions in addition to its previously established inhibitory role, and underscore the importance of fine-tuning the balance of BMP and MAPK signaling during development and in the adult.

Results

Generation of Smad1 mutant lines carrying point mutations

To generate the *Smad1^{C}* mutation, a targeting construct was designed to change the C-terminal SSVS motif into AAVA, in exon 7 (Fig. 1A; Hoodless et al. 1996; Kretzschmar et al. 1997b). Two correctly targeted embryonic stem (ES) cell clones were used to generate chimeras from which one transmitted this mutation (Fig. 1B). Western analysis of protein extracts from embryonic day 9.5 (E9.5) wild-type (wt) and *Smad1^{C}* mutants showed that this mutation did not affect protein levels (Fig. 1C).

For the *Smad1^{L}* mutation, the targeting construct incorporated serine-to-alanine substitutions in the MAPK-consensus phosphorylation sites and two conserved phosphoserines in exon 3 (Fig. 1D; see Materials and Methods for further discussion; Kretzschmar et al. 1997a). Two *Smad1^{L}* mutant mouse lines were established from correctly targeted ES cell clones (Fig. 1E), and both lines resulted in the same phenotype. Most of the analysis was done using *Smad1^{L}* line one. The Smad1L mutant protein was expressed at similar levels when compared with the wild-type protein (Fig. 1F).

Phenotypic consequences of the Smad1^{C} *mutation*

It has been shown that mutations in the Smad1 C-terminal end result in the absence of transcriptional activation upon BMP activation (Hoodless et al. 1996; Kretzschmar et al. 1997b). If Smad1 was to function exclusively downstream of BMP signaling, one prediction might be that the C-terminal mutation might lead to a phenotype identical to the loss of function. Intercrosses between *Smad1$^{C/+}$* animals failed to produce *Smad1$^{C/C}$* mutants at weaning (Table 1). Analysis of timed matings indicated that *Smad1$^{C/C}$* embryos were recovered in the expected Mendelian ratio until E9.5 (Table 1). *Smad1$^{C/C}$* embryos displayed posterior truncation, abnormal turning, and allantois malformation compared with wild-type specimens that are reminiscent of the *Smad1$^{-/-}$* mutants (Fig. 2A–D). *Smad1$^{C/-}$* mutants were similarly affected (data not shown). The allantois normally forms from the outgrowth of the extraembryonic mesoderm into the coelomic cavity (Downs et al. 2003). As for the *Smad1$^{-/-}$* embryos, failure of the allantois to connect to the chorionic plate and initiate placenta formation was the most likely cause of embryonic lethality in *Smad1$^{C/C}$* mutants (Fig. 2K–N; Lechleider et al. 2001; Tremblay et al. 2001; Hayashi et al. 2002). *Smad1$^{-/-}$* embryos are characterized by the presence of ectopic extraembryonic ectoderm as revealed by enhanced *Bmp4* and *Eomes* expression (Fig. 2F,I; Tremblay et al. 2001). The expression pattern of these markers in *Smad1$^{C/C}$* embryos showed a similar expansion of extraembryonic tissues compared with control embryos (Fig. 2E–J). These observations demonstrate that the development of extraembryonic structures relies on transcriptional activation of Smad1.

However, a closer examination of *Smad1$^{C/C}$* and *Smad1$^{-/-}$* embryos revealed disparities between both

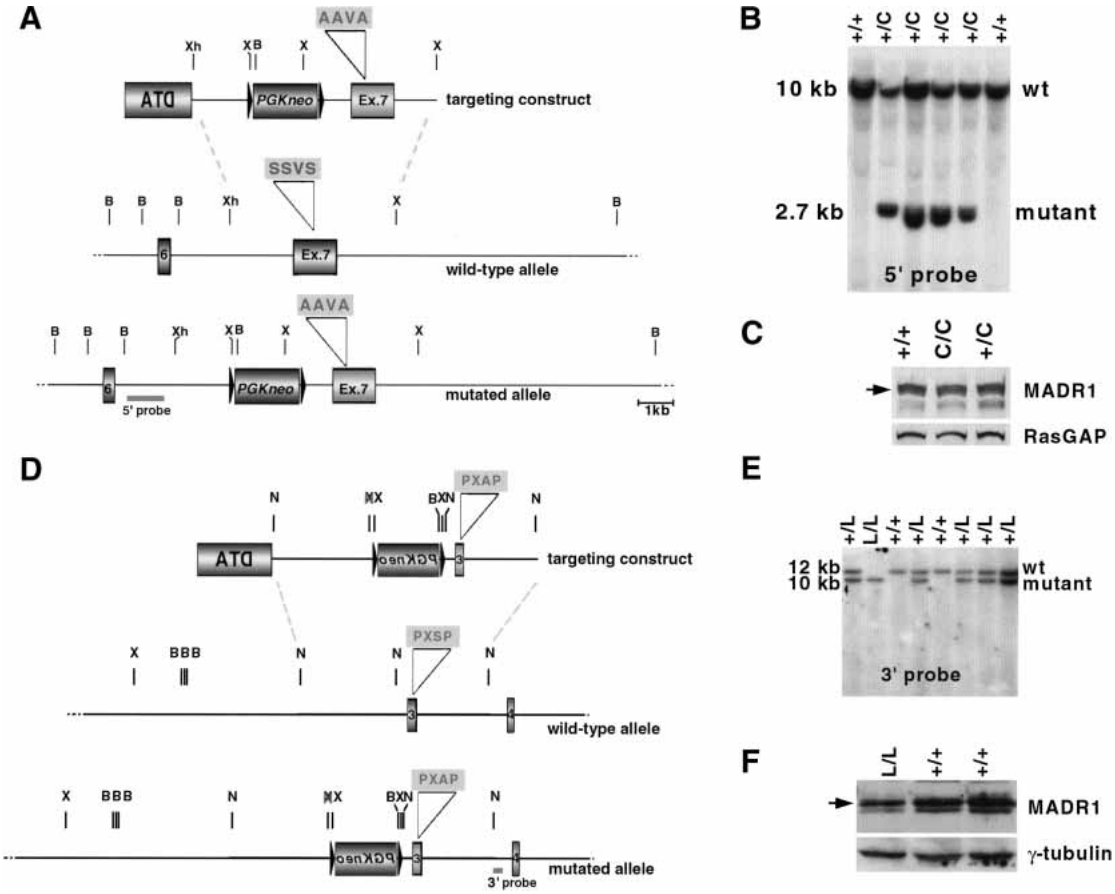

Figure 1. Targeting of the *Smad1* locus. (*A*) Introduction of mutations in the C-terminal end of the *Smad1* gene encoded by exon 7 using homologous recombination. The *PGKneo* selection cassette flanked by LoxP sites (arrowheads) and the diphtheria toxin (DTA) cassette in the targeting construct are indicated. (*B*) Southern blot analysis of DNA from ES cells using BamHI digestion hybridized with a 5′-flanking probe, to distinguish between the mutant (2.7 kb) and the wild-type (10 kb) alleles. (*C*) Western blot analysis of protein extracts from wild-type and *Smad1*^{C} mutant embryos showed that similar levels of Smad1 protein were detected for each genotype. RasGAP served as a loading control. (*D*) Introduction of the linker mutation by homologous recombination substituting a mutated exon 3. (*E*) Southern analysis using XbaI digestion and a 3′-flanking probe, to distinguish between the mutant (10 kb) and the wild-type (12 kb) alleles. (*F*) Western blot analysis of nuclear extracts from wild-type and *Smad1*^{L} mutant MEFs showed that similar level of Smad1 protein was detected for each genotype. γ-Tubulin was used as a loading control. (B) BamHI; (N) NheI; (X) XbaI; (Xh) XhoI.

phenotypes (Fig. 2B–D). In particular, anterior truncation of the head occurred in 7/8 *Smad1*$^{C/C}$ embryos. Furthermore, only one branchial arch was present, sometimes unilaterally (Fig. 2B,C). *Smad1*$^{C/C}$ embryos also displayed an enlarged pericardium and impaired development of the posterior aspects. These more severe phenotypes are likely due to defects in extraembryonic or primitive streak patterning at earlier stages and have not been observed in our cohort of null mutants (Fig. 2D) or reported so far (Lechleider et al. 2001; Tremblay et al. 2001). In contrast, allantois growth of several *Smad1*$^{C/C}$ embryos did not seem as severely impaired as in null mutants (Fig. 2M,N; Tremblay et al. 2001). Moreover, the allantois frequently fused at ectopic locations rather than at the chorionic plate (data not shown) and bulging allantois were rarely observed in contrast to *Smad1*$^{-/-}$ mutants (Fig. 2D). These results indicate that the C-terminal mutation results in phenotypes both more severe (e.g., anterior development) and less severe (allantois growth) than those reported for null mutants.

Table 1. *Genotypes of animals recovered from* Smadl^{C} *and from* Smadl^{L} *heterozygous intercrosses*

Age	No. of litters	Genotype		
		Smad1$^{+/+}$	*Smad1*$^{+/C}$	*Smad1*$^{C/C}$
E7.5	6	11 (33.3%)	13 (39.4%)	9 (27.3%)
E9.5	4	9 (23.7%)	19 (50%)	10 (26.3%)
Weaned animals	8	13 (30.2%)	30 (69.8%)	0 (0%)
		Genotype		
		Smad1$^{+/+}$	*Smad1*$^{+/L}$	*Smad1*$^{L/L}$
Weaned animals	27	55 (25.3%)	115 (53.0%)	47 (21.7%)

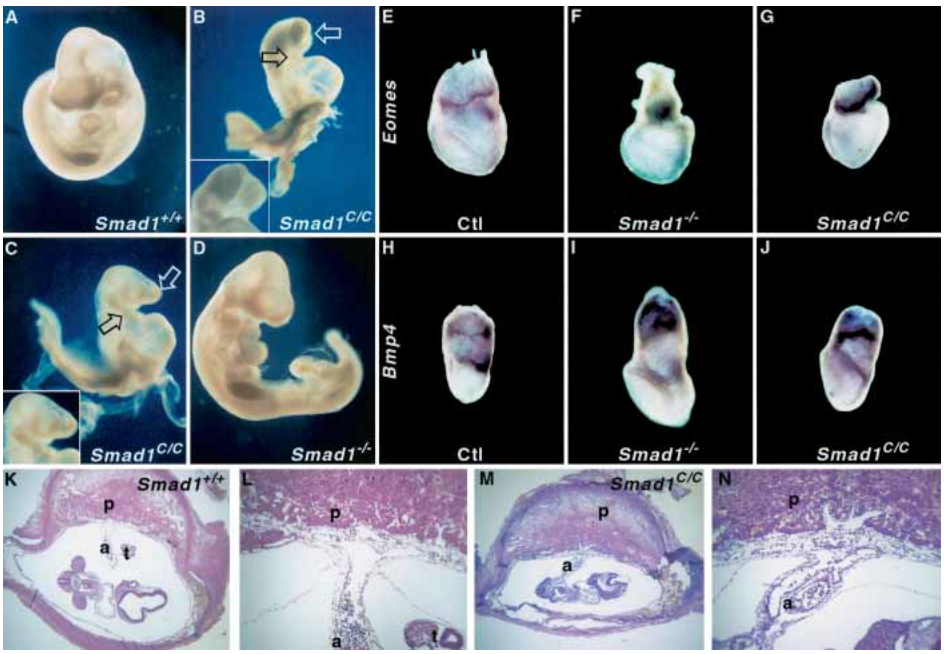

Figure 2. *Smad1*^{C} mutant phenotype. Comparison of E9.5 wild-type (*A*) and *Smad1*$^{C/C}$ (*B*,*C*) embryos showed that the C-terminal mutation caused heart defects, abnormal turning, and lack of ventral closure in the posterior region. Compared with the *Smad1*$^{-/-}$ (*D*), the *Smad*$^{C/C}$ (*B*,*C*) mutants also displayed head (open white arrow) and branchial arch (open black arrow) anomalies, showed in *insets*. (*E–J*) Whole-mount in situ hybridization analyses showed stronger *Eomes* expression in extraembryonic tissues of *Smad1*$^{-/-}$ (*F*) and *Smad1*$^{C/C}$ (*G*) embryos at E7.5, compared with controls (*E*). *Bmp4* expression was also abnormal in *Smad1*$^{-/-}$ (*I*) and *Smad1*$^{C/C}$ (*J*) mutants compared with the controls (*H*). The placental connection (*K–N*) was also defective in the *Smad1*^{C} mutants (*M*,*N*). In wild-type (*K*,*L*), the allantois fused to the placenta (*K*,*L*). In contrast, growth of the allantois was often observed (*M*) but either not properly fused in the *Smad1*^{C} mutants (*N*) or fused ectopically (data not shown). (a) Allantois; (p) placenta; (t) tail.

Phenotypic consequence of the Smad1^{L} *mutation on gastric homeostasis*

Breeding of *Smad1*$^{L/+}$ mice showed that the linker mutation did not affect viability, as *Smad1*$^{L/L}$ mutants were recovered at the expected frequency in heterozygous intercrosses at weaning (Table 1). TGFβ superfamily members are involved in the morphogenesis and homeostasis of several organ systems. To further investigate the potential role of Smad1 phosphorylation by MAPK-mediated signaling, adult animals were killed and various tissues were examined. With the exception of the reproductive tract of some *Smad1*$^{L/L}$ males (see below), no gross morphological anomalies were observed. Further attention was given to the digestive tract, as BMP signaling has been previously implicated in gut morphogenesis (Narita et al. 2000; Roberts 2000; Smith et al. 2000; Aubin et al. 2002). Histological analysis revealed that the cytology of the *Smad1*$^{L/L}$ gastric mucosa was perturbed (Fig. 3). The stomach of rodents consists of a proximal keratinized epithelium and a distal glandular mucosa (Gordon and Hermiston 1994). The glandular stomach is subdivided in three zones: a proximal zymogenic, a middle mucoparietal, and a distal pure mucus zone. In the zymogenic zone, the four main cell types show a stereotyped distribution: mucus-producing and zymogenic cells are found in the upper third and at the base of the unit, respectively, whereas parietal and enteroendocrine cells are distributed along the entire length. A common stem cell progenitor located in the isthmus repopulates each unit. In the *Smad1*$^{L/L}$ stomach, all the expected cell types were represented albeit with variations in their relative proportion (Fig. 3A–F). The zymogenic cells recognizable by their strong affinity for hematoxylin were severely depleted in linker mutants compared with wild-type samples (Fig. 3A–C). In addition, the parietal cells were more numerous in mutant compared with wild-type stomachs, as revealed by immunostaining with the H^+K^+ATPase proton pump antibody specific for this cell type (Fig. 3D,E). Mucous-producing and enteroendocrine cells were not substantially affected (data not shown). Stomach morphogenesis and primordial gastric unit formation was similar in wild-type and *Smad1*$^{L/L}$ mutants (tested at E13.5, E18.5, and postnatal day 0 [P0]; data not shown). The altered cellularity of *Smad1*$^{L/L}$ gastric epithelium was not associated with altered specification of the stomach epithelium into an intestinal identity, as revealed at P0 and in adults by the absence of alkaline phosphatase staining, a hallmark of intestinal transformation (Aubin et al. 2002; data not shown). Thus, preventing MAPK phosphorylation of Smad1 alters stomach homeostasis.

The reduction in zymogenic cells and the increased proportion of parietal cells indicated that cell specification in the *Smad1*$^{L/L}$ stomach was affected. Cell adhesion and migration are tightly controlled and correlate with cell differentiation in the gut (Gordon and Hermis-

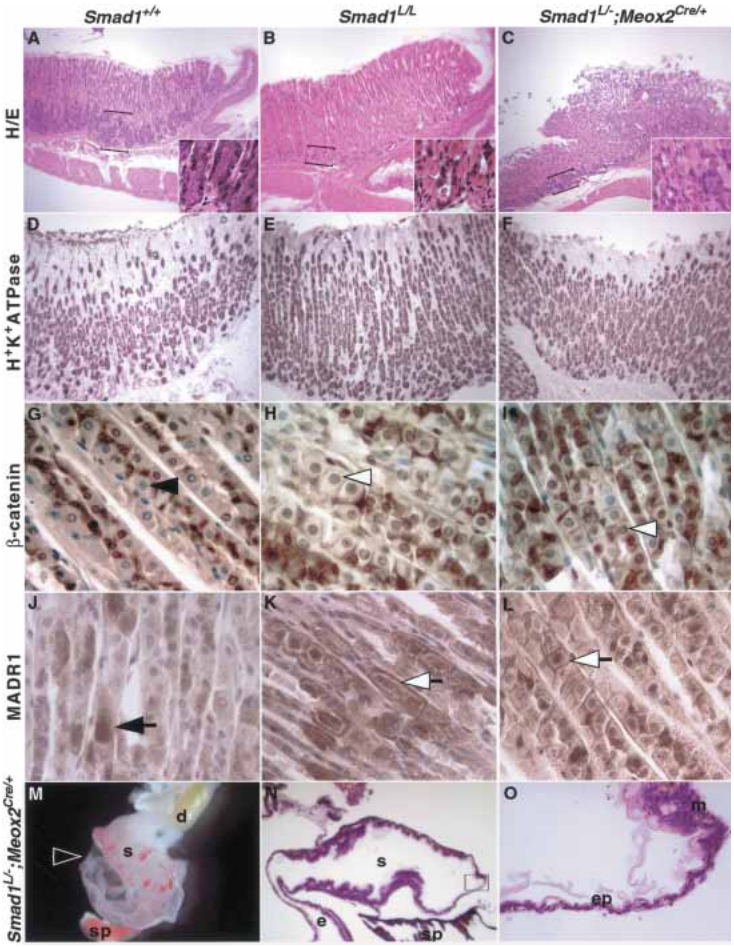

Figure 3. Stomach anomalies in *Smad1*^{L} mutants. Adult stomachs of wild-type (*A*,*D*,*G*,*J*), *Smad1*$^{L/L}$ (*B*,*E*,*H*,*K*), and *Smad1*$^{L/-}$; *Meox2*$^{Cre/+}$ mutants (*C*,*F*,*I*,*L*) were analyzed by histological (*A–C*) and IHC staining (*D–L*). HE staining revealed a decrease in the zymogenic cells (brackets), and an increase in parietal cells in *Smad1*^{L} mutants (*B*,*C*), compared with wild-type (*A*). (*A–C*, *insets*) Higher magnification of the zymogenic zone where parietal cells were abundant and zymogenic cells depleted in *Smad1*$^{L/L}$ and in *Smad1*$^{L/-}$; *Meox2*$^{Cre/+}$ mutants. The latter carry an *Smad1*^{L} allele in the context of the mosaic deletion of the null allele by *Meox2*$^{Cre/+}$-driven recombination. The increase in the number of parietal cells was clearly visible using an anti-H^+K^+ proton pump antibody specific for this cell type when comparing wild-type (*D*) with *Smad1*$^{L/L}$ and *Smad1*$^{L/-}$; *Meox2*$^{Cre/+}$ mutants (*E*,*F*). The latter carry a *Smad1*^{L} allele in the context of the mosaic deletion of the null allele by *Meox2*$^{Cre/+}$-driven recombination. (*C*) Furthermore, the gastric epithelium of *Smad1*$^{L/-}$; *Meox2*$^{Cre/+}$ mutants showed signs of disorganization. (*G–I*) Immunostaining using a β-catenin antibody revealed that parietal cells, recognizable by their "fried-egg" shape, showed increased proportion of nuclear staining (white arrowhead; *H*,*I*), compared with wild-type (black arrowhead; *G*). (*J–L*) Changes in the localization of Smad1 protein were also observed in mutants. In wild-type (*J*), Smad1 was distributed throughout the majority of parietal cells (black arrow), whereas a strong cytoplasmic membrane and nuclear staining were found in mutants (white arrow; *K*,*L*). Furthermore, a small proportion of *Smad1*$^{L/-}$ mosaic mutants died at birth from a ruptured stomach (open arrowhead; *M–O*). (*N*,*O*) Histology showed thinning of both the epithelial and the muscular layer and the absence of cardia at the junction of the esophagus and the stomach. (d) Duodenum; (e) esophagus; (ep) epithelium; (m) muscular layer; (s) stomach; (sp) spleen.

ton 1994). To further investigate changes in components of cell–cell adhesion, immunostaining was performed with a β-catenin antibody. In the majority of parietal cells, β-catenin was localized at the membrane (Fig. 3G–I). Although we could not unambiguously define if membrane-specific β-catenin labeling was modified in the *Smad1*$^{L/L}$ mucosa, enhanced β-catenin nuclear staining was observed in positively stained parietal cells when compared with wild-type controls (85.6% ± 4.7% vs. 63.4% ± 7.3%; $p < 0.01$). This observation suggests that Wnt signaling in the stomach might be influenced by the linker mutation.

To obtain further insights into the effect of the linker mutation, Smad1 protein localization was assessed in the gastric mucosa of wild-type and *Smad1*$^{L/L}$ adults. In wild-type mucosa, Smad1 was expressed at high levels in a subset of parietal cells, as previously reported (Fig. 3J–L; Huang et al. 2000). In most positive parietal cells, Smad1 was uniformly localized in the cytoplasm and in the nucleus. In contrast, Smad1 exhibited strong nuclear staining but cleared the cytoplasm and was localized at the cell membrane in *Smad1*$^{L/L}$ parietal cells (Fig. 3K,L). Preventing MAPK signaling through Smad1 in the gastric epithelium impinges on Smad1 protein distribution in parietal cells. This perturbed localization correlates with β-catenin nuclear accumulation and altered stomach homeostasis.

To examine if the *Smad1* linker mutation acts as a hypomorphic allele, we introduced the *Smad1*^{L} mutant allele over an *Smad1*-null background by crossing the linker mutants carrying the *Meox2*$^{Cre/+}$ deleter allele (Tallquist and Soriano 2000) with *Smad1* conditional null mice (Tremblay et al. 2001). In this context, 24% of the *Smad1*$^{L/-}$ pups died at birth (6/25; seven litters). These animals presented a bloated stomach and accumulation of air in the abdomen. The fragility of the stomach resulted in its rupture in severely affected newborns (Fig. 3M). Histology revealed that the muscular layer was almost completely absent and the epithelium was extremely thin (Fig. 3N,O). This increase in the severity of the stomach phenotype indicates that the *Smad1*^{L} mutation indeed behaves as a hypomorphic allele (Fig. 3C,M–O). We also crossed the linker mutants with *Smad5*$^{+/-}$ mice to test for potential functional redundancy by the closely and functionally related *Smad5* gene. *Smad5*$^{-/-}$ mutants die at midgestation of a complex set of phenotypes including vascular, gut, and ventrolateral morphogenesis defects, whereas *Smad5*$^{+/-}$ ani-

mals do not exhibit any phenotypes (Chang et al. 1999). Compound *Smad1*$^{L/L}$; *Smad5*$^{+/-}$ animals were recovered at the expected Mendelian frequency and did not present any overt phenotype, indicating that Smad5 does not play a compensatory role in *Smad1*$^{L/L}$ mutants. Taken together, these results demonstrate that MAPK and BMP cross-talk plays a significant role both in stomach morphogenesis and homeostasis.

Cellular consequences of the Smad1^{L} *mutation*

The relocalization of Smad1 protein in the parietal cells of the gastric epithelium in *Smad1*$^{L/L}$ mutants prompted further investigations in mouse embryonic fibroblast (MEF) lines. Accumulation of Smad1 at the membrane was observed in *Smad1*$^{L/L}$ but not in wild-type MEFs, similar to that observed in *Smad1*$^{L/L}$ parietal cells (Figs. 4A,B, 3J–L). Thus, preventing MAPK-mediated phosphorylation of the linker region resulted in abnormal localization of the Smad1 protein in at least two distinct cell types. To obtain independent verification that inhibiting MAPK signaling leads to Smad1 protein retention at the membrane, wild-type MEFs were treated with the MEK inhibitor U0126 and stimulated or not with platelet-derived growth factor (PDGF). Inhibiting MAPK signaling resulted in Smad1 retention at the membrane (Fig. 4J). Smad1 localization was not affected by the presence or absence of PDGF in control assays (Fig. 4I,J; data not shown). *Smad1*$^{L/L}$ MEFs were also characterized by tight cell–cell adhesion, as revealed by staining with a β-catenin antibody. In contrast to wild-type MEFs, in which cell–cell contacts were made through adhesion zippers (Fig. 4C), *Smad1*$^{L/L}$ cells displayed stronger intercellular contacts as evidenced by the flat staining pattern between cells (Fig. 4D). Staining with a cadherin-specific antibody correlated with that observed with β-catenin (Fig. 4E,F). The actin cytoskeleton of *Smad1*$^{L/L}$ MEFs was characterized by accumulation of cortical actin and a decrease in stress fibers compared with wild-type cells (Fig. 4G,H). Furthermore, the morphological change in cell shape of *Smad1*$^{L/L}$ MEFs was reflected by the accumulation of focal adhesions at the periphery of the cell (data not shown). Similar results were obtained for at least two different MEF lines from each genotypes. Thus, at physiological levels, MAPK signaling influences Smad1 cellular localization in MEFs, as observed in stomach parietal cells, and preventing Smad1 linker phosphorylation affects several cellular characteristics.

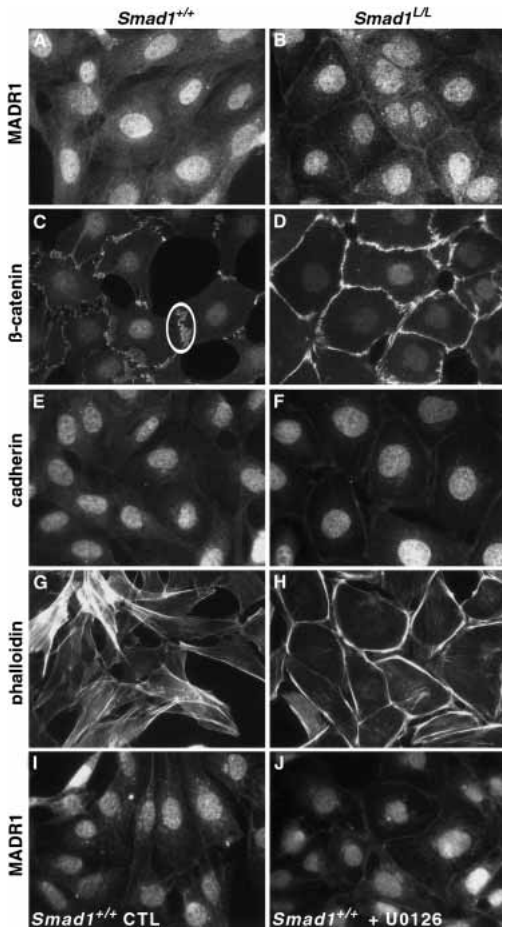

Figure 4. Characterization of *Smad1* mutant MEFs. Immunofluorescence analyses showed redistribution of Smad1 protein in *Smad1*$^{L/L}$ MEFs (*B*) compared with wild-type (*A*). Staining at the membrane was stronger in the former. β-Catenin staining indicated that *Smad1*$^{L/L}$ cells lose adhesion zippers (*D*) normally observed in wild-type cells (circle; *C*) and exhibit increased cadherin staining at the membrane (*E*,*F*). Relocalization of actin to the cortex and reduction in stress fibers were predominant in *Smad1*$^{L/L}$ MEFs (*H*), in contrast to wild-type cells (*G*). In wild-type MEFs stimulated with PDGF, treatment with the MAPK inhibitor U0126 (*J*) caused retention of the Smad1 protein at the membrane. This pattern was not observed in control conditions (*I*; data not shown).

Effect of Smad1^{L} *and* Smad1^{C} *mutations on germ cells*

TGFβ superfamily members regulate development of PGCs and the morphogenesis of the reproductive tract (Behringer et al. 1994; Mishina et al. 1996; Allard et al. 2000; Jamin et al. 2000; Tremblay et al. 2001; Chang and Matzuk 2001; Hayashi et al. 2002; Pellegrini et al. 2003). In the mixed (129S4/C57BL/6) genetic background, intercrosses between *Smad1*$^{L/L}$ mutants tended to be less productive than those between *Smad1*$^{L/+}$ animals (3.75 ± 2.36 vs. 8.00 ± 2.03 pups/litter, respectively; $p < 0.001$). Adult wild-type and *Smad1*$^{L/L}$ animals were killed, and gross morphological examination revealed that 2/7 *Smad1*$^{L/L}$ males had smaller testes and abnormal reproductive tracts (Fig. 5A–D). Histological analyses showed that affected *Smad1*$^{L/L}$ testis cords were disorganized and depleted of primordial germ cells (PGCs; Fig. 5D). We next examined the presence of PGCs in E13.5 embryos by alkaline phosphatase (AP) activity. AP staining showed that whereas PGCs were present in some *Smad1*$^{L/L}$ mutant gonads, others lacked them entirely (Fig. 5G–J). This phenotype was not sex-specific as both males (Fig. 5C,D) and females (Fig. 5I,J) were affected. To test if the lack of PGCs in E13.5 gonads could

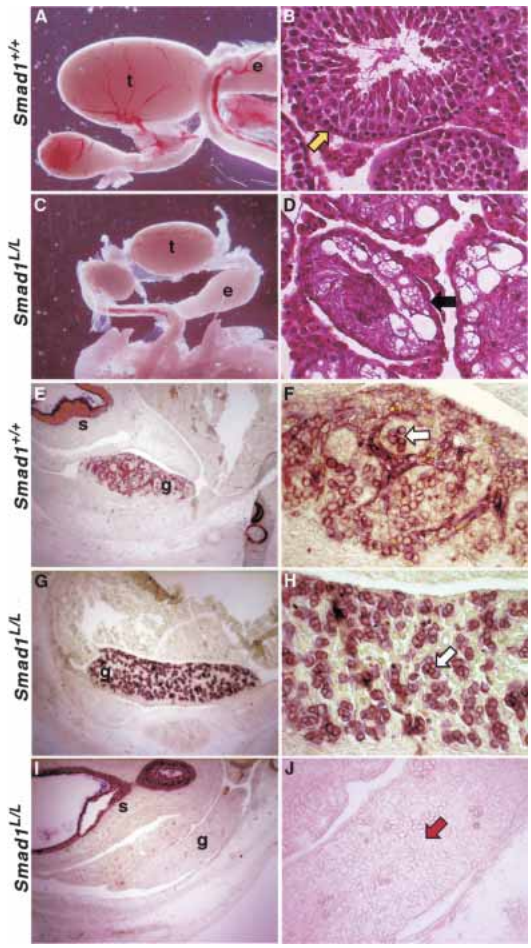

Figure 5. Reproductive defects in *Smad1*$^{L/L}$ mutants. Gross morphology of the male reproductive tract (*A*,*C*) revealed smaller testes and abnormal epididymis in *Smad1*$^{L/L}$ males (*C*) compared with wild-type (*A*). Upon histology, the testis cord was disorganized in affected *Smad1*$^{L/L}$ mutants compared with controls (data not shown). Furthermore, whereas PGCs were readily detectable at the periphery of wild-type testis cord (yellow arrow; *B*), they were severely depleted in affected *Smad1*$^{L/L}$ males (black arrow; *D*). Sertoli cells were unaffected. (*E–J*) AP staining on gonad sections of E13.5 embryos showed that PGCs were strongly labeled (white arrow) in wild-type (*E*,*F*) and in a proportion of *Smad1*$^{L/L}$ mutants (*G*,*H*), whereas other *Smad1*$^{L/L}$ gonads were devoid of germ cells (red arrow; *I*,*J*). (e) Epididymis; (g) gonad; (s) stomach; (t) testis.

be due to defects in the emergence of this cell population at gastrulation, whole-mount AP staining was performed on E7.5 embryos, and PGCs were counted. At this time, PGCs are normally readily detectable at the base of the allantois. Of the *Smad1*$^{L/L}$ mutants, 60% (n = 15) had a low PGC count (<15 PGCs per embryo; Fig. 6B,E). Thus, the decreased fertility of *Smad1*$^{L/L}$ animals is most likely caused by a defect in the emergence of PGCs early in embryonic development, indicating a further role for phosphorylation of the Smad1 linker region.

In *Smad1*$^{-/-}$ embryos, PGCs are not formed, whereas *Smad1*$^{+/-}$ animals are hypofertile because of a decrease in PGCs, most likely reflecting a dosage effect (Tremblay et al. 2001; Hayashi et al. 2002). In contrast, *Smad1*$^{C/+}$ mutants displayed normal fertility. Taking into account the fact that homozygous mutants derived from *Smad1*$^{C/+}$ heterozygous matings are lethal, the number of pups recovered in this type of cross (5.4 ± 2.7 pups/litter) was similar to that expected (6 pups/litter on average). We also observed that all E7.5 *Smad1*$^{C/C}$ embryos (n = 9) tested were almost completely devoid of PGCs (Fig. 6C,E), confirming that the emergence of the germ-cell lineage was dependent on the transcriptional activity of Smad1, most probably in response to extraembryonic BMP4, BMP8b, and embryonic BMP2 signals (Lawson et al. 1999; Ying et al. 2000; Fujiwara et al. 2001; Tremblay et al. 2001; Ying and Zhao 2001; Hayashi et al. 2002). Because *Smad1*$^{C/+}$ mutants are not as severely

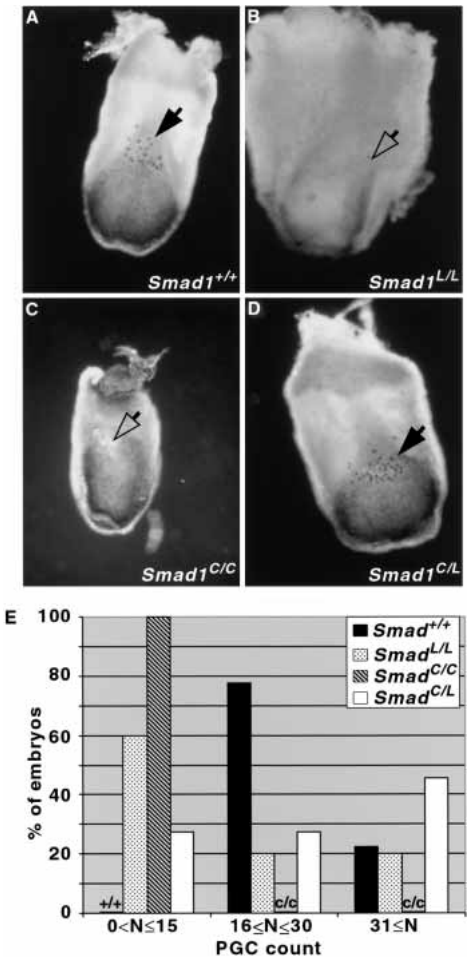

Figure 6. PGC formation at E7.5 in wild-type, *Smad1*^{L}, and *Smad1*^{C} mutants. E7.5 embryos were stained for AP (*A–D*) to detect PGC at the posterior side of the wild-type (*A*), *Smad1*$^{L/L}$ (*B*), *Smad1*$^{C/C}$ (*C*), and *Smad1*$^{C/L}$ (*D*) embryos. Compared with the number of PGCs observed in wild-type embryos (black arrow, *A*), some *Smad1*$^{L/L}$ mutants (*B*) and almost all *Smad1*$^{C/C}$ embryos (*C*) were depleted of PGCs (open arrow). PGC formation was restored in *Smad1*$^{C/L}$ mutants (black arrow; *D*). (*E*) The modal distribution of embryos according to their genotype and the PGC count is shown. Embryos were classified in three categories depending on the number of PGCs.

affected as $Smad1^{+/-}$ animals, this may indicate that the mutant protein contributes to restoring the fertility in a BMP-independent manner.

Because both the linker and the C-terminal mutation led to a reduction in PGC numbers, although much more severe for the $Smad1^{C/C}$ mutants, we next asked if the formation of PGCs was also affected in $Smad1^{C/L}$ compound mutants, as signaling from both MAPK and BMPs could still occur. Intercrosses of $Smad1^{C/L}$ heterozygous mice with either $Smad1^{C/L}$ or $Smad1^{C/+}$ animals indeed produced as many pups (8.25 ± 2.49 pups/litter, 12 litters) as $Smad1^{L/+}$ or wild-type breeding (8.00 ± 2.03 pups/litter, 27 litters), despite the lethality of $Smad1^{C/C}$ mutants. Accordingly, the number of PGCs formed in E7.5 $Smad1^{C/L}$ embryos (n = 11) was normal in the majority of the embryos examined (Fig. 6D,E). Furthermore, the recovery of $Smad1^{C/C}$ embryos in the expected proportion did not support the notion of a bias in allelic transmission (data not shown). Therefore, the rescue observed in PGC formation by the linker and C-terminal mutations suggests complementation between $Smad1^{L}$ and $Smad1^{C}$ alleles, and that MAPK as well as BMP signaling through Smad1 are required for the emergence of the germ line.

Discussion

Smad1 as a mediator of BMP signaling

The introduction of the C-terminal mutation in the $Smad1^{C}$ mouse line provides a means to evaluate if Smad1 function depends entirely on its transcriptional activation by BMP signaling, by comparing the resultant mutant phenotype to that of the null mutation. Preventing phosphorylation of the C-terminal residues led to several phenotypes similar to the loss-of-function mutation, with defects in the posterior structures of the embryo, in PGC development, and in development of extraembryonic mesoderm (Figs. 2, 6; Tremblay et al. 2001). However some of the defects in extraembryonic structures—for example, allantois growth—appeared less severe than those observed with the null allele. Such a result might be expected if not all Smad1 activities are dependent on transcriptional activation by BMP signaling.

$Smad1^{C/C}$ embryos have additional head and branchial arch anomalies not observed in $Smad1^{-/-}$ mutants (Fig. 2). A role for BMP in anterior development is illustrated by the analysis of *Bmp4* mouse mutants also carrying a mutation in *Twisted gastrulation*, thought to act as a pro-BMP factor in the head region (Zakin and De Robertis 2004). One possible explanation for the enhanced severity of our phenotype is that the $Smad1^{C}$ exerts a dominant-negative effect on BMP signaling by interfering with *Smad5*-mediated signaling. Consistent with this interpretation, the anterior truncation we observe appears similar to that seen in $Smad5^{-/-}$ mutant embryos (Chang et al. 1999). A putative dominant effect could be due to the competition between wild-type and the Smad1C proteins for a putative receptor-associated recruiting protein. Alternatively, the Smad1C protein may interfere with kinetics of activation at the receptor level, hampering the recruitment of Smad5 and Smad8 to the receptor complex. Consistent with this hypothesis, the interaction between the receptor kinase complex and R-Smads has been shown to be stronger when the R-Smad C-terminal phosphorylation sites are mutated (Qin et al. 2001).

On the other hand, some experimental data do not support the notion of a dominant-negative effect. For instance, the presence of the Smad1C protein does not have a deleterious effect on the fertility of heterozygous animals, as might be expected if it acted as a dominant negative. Moreover, in *Xenopus* embryos, a C-terminal mutant Smad1 protein has only a weak, if any, ventralizing effect (Pera et al. 2003). Consequently, embryonic structures in $Smad1^{C/C}$ mutants showing enhanced severity of the C-terminal mutation compared with the nulls may represent sites that require a strict equilibrium between BMP and MAPK inputs (e.g., anterior formation). Less severe phenotypes (e.g., allantois growth) would rather reflect sites of BMP-independent functions for Smad1.

Smad1 as a mediator of MAPK signaling

The analysis of the Smad1 linker phenotype provides the first evidence for a role of integrating BMP and MAPK signaling in epithelial homeostasis. Rendering the Smad1 protein resistant to MAPK-mediated phosphorylation alters homeostasis of the gastric epithelium as reflected by the increased parietal cells and decreased zymogenic cell populations (Fig. 3). Our characterization provides some hints on how MAPK signals affect homeostasis via Smad1. As we and others (Huang et al. 2000) have shown, Smad1 is expressed at high levels in parietal cells, a cell population that is expanded in $Smad1^{L/L}$ mutants (Fig. 3H,I). Parietal cell depletion experiments in transgenic mice have demonstrated that this cell type influences decision-making among gastric epithelial cell precursors and modulates the migration-associated terminal differentiation programs of the pit (mucous-producing) and zymogenic lineages (Li et al. 1996). Changes in the parietal cell population in $Smad1^{L/L}$ mutants are therefore most likely to impede this migration-associated differentiation and underlie the perturbed homeostasis. However, we cannot exclude a cell-autonomous role in the differentiation of zymogenic cells because Smad1 is also expressed at low levels in these cells (Huang et al. 2000; J. Aubin and P. Soriano, unpubl.).

A regulatory role for MAPK signaling in epithelial homeostasis is further supported by the consequence on gastric homeostasis of overexpressing activated K-ras in the stem cell region (isthmus) of the gastric epithelium (Brembeck et al. 2003). Overactive K-Ras leads to a decrease in parietal cells, a phenotype opposite to that seen in $Smad1^{L/L}$ mutants. It would be worth testing if the Smad1L protein could rescue some aspects of the activated K-ras phenotype. Rescue of the effect of activated Ras has indeed been reported in cultured colon cancer cells by a linker mutant (Ras-resistant) form of Smad3 (Calonge and Massagué 1999).

An additional factor that may contribute to altered functional specification of the stomach is the enhanced β-catenin nuclear staining, suggesting activated Wnt signaling. How both BMP and Wnt signaling are intertwined in this organ system remains to be addressed, but one interesting possibility is that Smad1 and β-catenin might directly interact in parietal cells. Such a direct association has been observed in kidneys of ALK3 transgenic mice and in wild-type MEFs (Hu et al. 2003; J. Aubin and P. Soriano, unpubl.).

The severity of the stomach alteration in some of the $Smad1^{L/-}$ mutants unveils the importance of fine-tuning BMP signaling during organogenesis. Stomach morphogenesis is known to rely on several signaling cascades, and requires integration of TGFβ and FGF signals (Aubin et al. 2002). The source of MAPK signaling that is involved in this process remains to be identified, but FGF10 and its cognate receptor FGFR2b constitute potential candidates. The glandular stomach is particularly sensitive to the action of BMP and FGF signaling as they are both essential for its formation (Fig. 3M–O; Narita et al. 2000; Smith et al. 2000). This potential scenario is reminiscent of the role of FGF/IGF signaling in antagonizing BMP action in neural development in *Xenopus* (Pera et al. 2003). The extent of the defect on both the epithelium and the muscular layer in $Smad1^{L/-}$ stomach, however, may indicate that cell autonomous as well as non-cell-autonomous factors are involved in this phenotype.

We expected the mutation of the linker phosphorylation sites to lead to nuclear accumulation, based on work in cell lines that pointed to the nuclear exclusion of Smad1 upon MAPK activation. This event, however, depends on the cell type and may be more perceivable in an oncogenic context (e.g., hyperactive Ras; Kretzschmar et al. 1997a, 1999; Massagué 2003). Instead at physiological levels, the Smad1L protein was found to clear the cytoplasm and is retained at the plasma membrane in MEFs and parietal cells. An important function of MAPK-mediated linker phosphorylation might thus be to prevent undesired Smad1 retention at the membrane, which could lead to altered cell adhesion and cytoskeletal remodeling.

Changes observed in the cytoskeletal organization raise the question of a putative direct involvement of Smad1/BMP signaling in actin reorganization. Recently, BMP signaling has been shown to influence actin dynamics by regulating the activity of LIMK1, a kinase that phosphorylates the actin cytoskeleton regulator cofilin (Foletta et al. 2003). Further experiments are needed to address the effect of membrane-localized Smad1L protein on LIMK1 regulation.

Smad1 as a convergence point for multiple signaling pathways

A developmental process greatly affected by the differential phosphorylation of Smad1 is the formation of the germ-cell lineage. The requirement of Smad1 transcriptional activity for PGC formation was expected based on the null mutant phenotype, but the decreased PGC population in the linker mutant was more surprising. In MEFs, the linker mutation was found to stabilize β-catenin and cadherin at the membrane and enhance homophilic interactions (data not shown). E-Cadherin-mediated interactions in PGC precursors are required for their fate and commitment to the germ-cell lineage (Okamura et al. 2003). How E-cadherin regulates PGC determination remains to be determined, but one hypothesis is that E-cadherin could function as an anchor that settles precursor cells within niches for PGC differentiation. This scenario would be similar to the role of DE-cadherin in the *Drosophila* ovary, where the BMP homolog decapentaplegic (dpp) is responsible for the clonal expansion of the germ-cell lineage (Zhu and Xie 2003). Changing the balance in cell–cell interactions might thus jeopardize PGC formation in $Smad1^{L/L}$ mutants. In compound mutants, Smad1C might rescue germline precursors by restoring normal cell–cell contacts perturbed by the Smad1L mutant protein. Further tests of this hypothesis will require analysis of cell adhesion in PGC precursors, and identifying the relevant source of MAPK signaling regulating germ-cell development.

The integration of Smad and MAPK pathways has been recently examined in *Xenopus* embryos (Grimm and Gurdon 2002; Pera et al. 2003). IGF, FGF, and anti-BMP signals were found to mediate differential Smad1 phosphorylation and synergize in neural induction, and introduction of a linker mutant Smad1 resulted in embryo ventralization (Pera et al. 2003). In contrast, the *Smad1* linker mutation in the mouse leads to a less dramatic phenotype. One factor that may account for the mild outcome of the $Smad1^{L}$ mutation is that its effect when expressed at physiological levels may be masked by the compensatory action of Smad5 and Smad8, whereas this may not be the case in the *Xenopus* overexpression studies. Our attempt to test this by generating $Smad1^{L/L}$; $Smad5^{+/-}$ mutants did not reveal any additional obvious defects. Smad1 and Smad5 are highly identical at the amino acid level (<90%), and all MAPK-consensus sites in the linker region are conserved between both proteins. It is thus possible that the total amount of Smad1, Smad5, and possibly Smad8 proteins phosphorylated as a result of MAPK signaling defines the final balance between BMP and RTK signaling in the mouse. Consequently, developmental processes in which the genes are differentially expressed, such as in PGC formation (Hayashi et al. 2002), would be more sensitive to the linker mutation. Further reducing the threshold of the MAPK-phosphorylated Smad pool, as in $Smad1^{L/-}$; $Smad5^{+/-}$ compound mutants, or generating $Smad1^{L/L}$; $Smad5^{L/L}$; $Smad8^{L/L}$ triple linker mutants might be required to further define the cellular outcome of BMP/RTK cross-talk.

Taken together, our study underscores the importance of fine-tuning the balance of BMP and MAPK signaling through Smad1 in a physiological context. The unforeseen germ-cell and gastric epithelial phenotype, as well as the cellular consequences of the linker mutation, raise interesting questions about the underlying mechanisms

of BMP-MAPK cross-talk. They also support the notion that MAPK-dependent Smad1 phosphorylation may not only serve to inhibit BMP signaling but may serve other important cellular functions as well. An outstanding issue remains to identify the source of MAPK signaling in affected tissues. Another interesting aspect is how Smad1 linker phosphorylation impinges on Wnt signaling through β-catenin. The *Smad1^C* and *Smad1^L* mutant lines provide useful tools to tackle these questions and to further dissect the functional significance of integrating diverse signaling pathways.

Materials and methods

Mutagenesis of the Smad1 *gene*

Two *Smad1*-specific clones, p*12.7* and p*25.2* encompassing exon 3 and exon 7, respectively, were isolated from a λ phage 129S4 genomic library and used to generate the point mutant targeting vectors. To introduce the appropriate mutations, exon 3 and exon 7 subclones derived from the genomic library were subjected to 18 PCR cycles using PfuI polymerase and mutated oligonucleotides (Table 2), followed by DpnI digestion to eliminate the wild-type parental vector. Properly mutagenized clones were identified based on diagnostic restriction sites introduced by the mutagenesis and verified by sequencing. A diphtheria toxin-A cassette was included for negative selection (Fig. 1). For the C terminus mutation (*Smad1^C*), serine-to-alanine substitutions were introduced in exon 7 of the *Smad1* gene (S455A, S456A, and S458A; Kretzschmar et al. 1997b). Regarding the linker mutation, at the time this work was initiated, Kretzschmar et al. (1997a) had identified several residues in the linker region of the Smad1 protein that were potential phosphorylation targets, in addition to the four Erk-consensus motifs (S187, S195, S206, and S214). These additional residues included S209 and S210, as well as a stretch of four serines followed by a threonine (S198, S199, S200, S201, and T202). Examination of the closely related Smad5 homolog showed that all four Erk-consensus sites as well as S209 and S210 were conserved in both proteins, whereas this was not the case for S198, S199, S200, S201, and T202. This observation, along with the fact that residual basal Smad1 phosphorylation still occurred when the PXSP motifs were mutated (Kretzschmar et al. 1997a), prompted us to introduce serine-to-alanine substitutions in the MAPK consensus motifs (S187A, S195A, S206A, and S214A) as well as in S209 and S210. The innocuous character of S209 and S210 mutations on BMP-responsiveness was confirmed by comparing *Smad1$^{L/L}$* and wild-type MEFs using the three following criteria: (1) transcriptional profiling of downstream targets by microarray analysis; (2) induction of known transcriptional targets by Northern analyses (e.g., *Smad7*, *Id1*, and *Id3*); and (3) kinetics of activation of Smad1wt and linker mutant proteins. Similar results were obtained for both genotypes in all of the above experiments (data not shown).

AK7 ES cells were electroporated with the linearized vectors and selected for 10 d in 300 μg of G418 (total powder) per milliliter. PCR was used to identify ES colonies with targeted alleles. Positive colonies were analyzed by Southern blot to confirm the correct recombination events for each gene targeting prior to injection into blastocysts. The *PGKneo* selection cassette flanked by LoxP sites was removed from *Smad1^L* and *Smad1^C* lines by crossing the mutants with the *Meox2^{Cre}* deleter line (Tallquist and Soriano 2000). This deleter line was also used for the total ablation of the *Smad1* allele in the *Smad1* conditional null mouse line (provided by Liz Roberston, Harvard University, Cambridge, MA; Tremblay et al. 2001). The *Smad5* mutant line was obtained from Marty Matzuk (Baylor College of Medicine, Houston, TX; Chang et al. 1999). The presence of the *PGKneo* selection cassette did not affect either the *Smad1^L* or *Smad1^C* phenotypes (data not shown). The *Smad1^L* and *Smad1^C* mutations were analyzed in mixed (C57BL/

Table 2. *Oligonucleotides used for mutagenesis and genotyping*

Name (strand)	5′-Sequence-3′[a]	Use
JA14 (+)	GGGCTCACCCCACAATCCTATT**G**C**CG**C**G**GTG**G**CTTAAAAGA CCTGTGGCTTCCG	Mutagenesis *Smad1^C*
JA15 (–)	CGGAAGCCACAGGTCTTTTAAG**C**CAC**C**G**CG**G**C**AATAGGATT GTGGGGTGAGCCC	Mutagenesis *Smad1^C*
JA16 (+)	CCCGTTCCCCCAC**G**CCCCCAACAGCAGCT	Mutagenesis *Smad1^L* site A
JA17 (–)	AGCTGCTGTTGGGGG**C**GTGGGGGAACGGG	Mutagenesis *Smad1^L* site A
JA18 (+)	CAGCAGCTACCCCAAC**G**CTCCTGGCGGCAGC	Mutagenesis *Smad1^L* site B
JA19 (–)	GCTGCCGCCAGGAG**C**GTTGGGGTAGCTGCTG	Mutagenesis *Smad1^L* site B
JA20 (+)	GCAGCAGCACCTACCCTCAC**G**CCCCAACC**GCTG**CAGACCC GGGCAGCCC	Mutagenesis *Smad1^L* site C+D PstI site
JA21 (–)	GGGCTGCCCGGGTCTG**CAGC**GGTTGGGG**C**GTGAGGGTAGG TGCTGCTGC	Mutagenesis *Smad1^L* site C+D
JA22 (+)	GCAGACCCGGG**AGCT**CCTTTTCAGATGCCAG	Mutagenesis *Smad1^L* site E
JA23 (–)	CTGGCATCTGAAAAGG**AGCT**CCCGGGTCTGC	Mutagenesis *Smad1^L* site E
JA65C (+)	ACTCAGATGTCAGCAGACTGTCAG	*Smadl^L* genotype WT + mutant alleles
LmutAS (–)	CAACTGTCAATTCCACAGTACTGAC	*Smadl^L* genotype WT + mutant alleles
Lox (–)	ACGAAGTTATTAGGTCCCTCGAC	Genotype *Smadl^L* + *Smad1^C* alleles
CmS (+)	GTCAGGCTCCATCATTCATCTGG	Genotype WT + *Smad1^C* alleles
CmAS (–)	CTAAAGAGACAGACCTGCATAATAACTG	Genotype WT + *Smad1^C* alleles
SlCAFA (+)	TTGGTCCCTGCCTCTGCTCTCCAGTC	Genotype WT + *Smad1$^-$* alleles
S1CARA (–)	TAGCCATTATCAGAAGTCACCCTTGG	Genotype WT + *Smad1$^-$* alleles
S1CARB (–)	TACTATGTGATGGCGTAATGTTATC	Genotype *Smad1$^-$* allele

[a]Mutations are indicated in underlined, bold letters.

6;129S4) and in congenic 129S4 genetic backgrounds, with no difference in the phenotypic outcome. Analyses were done mainly on animals on a mixed genetic background. PCR oligonucleotides for the genotyping of the different mouse lines are listed in Table 2, except for the *Smad5* mutant line, which was genotyped by PCR as described (Chang et al. 1999).

Tissue collection, immuno- and histochemical analyses

Tissues from wild-type and *Smad1* mutant animals killed at different times after birth were collected in ice-cold phosphate-buffered saline (PBS). For the gut, different portions were subdivided prior to fixation in cold 4% paraformaldehyde (PFA) in PBS, followed by dehydration and paraffin embedding. Embryos at different stages of development were also harvested and processed for histology. Sections (6 µm) were stained with hematoxylin and eosin (H/E) or processed for immunohistochemistry (IHC) according to standard procedures.

PGC detection was performed by incubating rehydrated sections (for E13.5) or E7.5 embryos with NBT (Nitroblue Tetrazolium Chloride)/BCIP (5-bromo-4-chloro-3-indolylphosphate p-Toluidine; Life Sciences) substrate to detect AP activity.

Antibodies

The antibodies used in IHC, Western, and immunofluorescence (IF) experiments include an anti-MADR1 rabbit polyclonal antibody (Rab; Chemicon) to detect Smad1; an H^+/K^+ATPase mouse monoclonal antibody (Mab; Sigma) specific for parietal cells; a β-catenin Rab (Sigma); anti-E/N-cadherin Rab (provided by V. Vasioukhin, Fred Hutchinson Cancer Research Center, Seattle, WA); an anti-phospho-specific Smad1/5/8 Rab (Cell Signaling Technology); a goat anti-mouse γ-tubulin antibody (Santa-Cruz); and an anti-RasGAP (70.3) Rab that was a crude polyclonal antisera raised against a GST fusion protein. The identity of the Smad1 band detected by the MADR1 antibody was confirmed in control experiments using extracts from Smad-1 overexpressing as well as Smad-1 null cells. Secondary antibodies were horseradish peroxidase-conjugated donkey anti-rabbit IgG or biotinylated goat anti-rabbit/anti-mouse IgG polyclonal antibodies (Vector Laboratories).

In situ hybridization analyses

The whole-mount in situ hybridization protocol was performed as described in Wilkinson and Nieto (1993). The following murine fragments were used as templates for synthesizing digoxigenin-labeled riboprobes: a 1-kb SmaI–EcoRI fragment containing 5′ noncoding and coding sequences from the *Bmp4* gene (provided by Brigid Hogan, Duke University, Durham, NC); a *Eomesodermin* cDNA probe (*Eomes*; provided by Jean Charron, Université Laval, Quebec, Canada).

Cell culture and immunofluorescence analysis

MEF lines were established from E13.5 $Smad1^{+/+}$ and $Smad1^{L/L}$ embryos. Embryos were trypsinized and plated on gelatin-coated plates. Cell lines were established by splitting them approximately once every 3 d. For $Smad1^{-/-}$ MEFs, cells were derived from E9.5 embryos (provided by Liz Roberston) and were transformed by infection using supernatant from an SV40 retroviral producing line (Berghella et al. 1999). Control wild-type MEFs were also established in parallel.

For immunofluorescence analysis, trypsinized cells were plated on poly-L-lysine-coated coverslips and cultured overnight. Cells were fixed in 2% PFA in PBS for 10 min, followed by three washes in PBS 0.1% Triton. Cells were incubated for 1 h with primary antibodies. After three washes, cells were incubated with the appropriate secondary antibodies, washed again, and mounted in aqueous medium.

For MAPK inhibitor treatment, MEFs were plated on coverslips and put to rest the next day by culturing them in low serum medium condition for 24 h. They were then treated either with DMSO (control) or 10 µM U0126 (Calbiochem) for 1 h. Following stimulation with 10 ng/mL Platelet-derived Growth Factor for 30 min., cells were fixed and immunofluorescence was performed as described above.

Western blot analyses

E9.5 embryos and plated cultured cells were lysed in RIPA lysis buffer (50 mM Tris-HCl at pH 8.0, 150 mM NaCl, 1% NP-40, 0.5% sodium deoxycholate, 0.1% sodium dodecyl sulfate) containing 1 mM PMSF, 1 mM sodium orthovanadate, and 10 µg/mL proteinase inhibitor cocktail (Roche). Total cell lysates were incubated on ice for at least 15 min and centrifuged, and the supernatant was transferred to a clean tube. Protein content was quantified using a protein bioassay reagent (Bio-Rad), and 50 µg was loaded for analysis by SDS-PAGE. Proteins were electrotransferred onto a nitrocellulose membrane (Amersham). Incubation with recommended antibody dilutions was done overnight at 4°C.

Nuclear extracts were prepared as follow. Trypsinized cells (10-cm plates) were washed with cold PBS and transferred to a microfuge tube. After a brief centrifugation, cells were washed in 1 mL of Buffer A (10 mM HEPES at pH 7.9, 1.5 mM $MgCl_2$, 10 mM KCl, 0.5 mM DTT, 2 mM PMSF, 2 mM sodium orthovanadate), resuspended in 1 mL of Buffer A, and set on ice for 10 min to swell and lyse cells. Lysis was verified under microscope examination. After vigorous mixing, the lysate was spun down briefly. The pellet was resuspended in equal volume of Buffer C (10 mM HEPES at pH 7.9, 420 mM NaCl, 15 mM $MgCl_2$, 0.2 mM EDTA, 0.5% DTT, 5 mM PMSF, 2 mM sodium orthovanadate, 25% glycerol) and set on ice for 15 min. Nuclear extracts were spun at 13,000 rpm for 10 min at 4°C. Aliquots were frozen at −70°C until used for protein quantitation and Western blot analysis.

Acknowledgments

We thank Liz Robertson for providing *Smad1* cDNA clones, $Smad1^{-/-}$ MEFs, and the Smad1 conditional null mice; Marty Matzuk for the *Smad5* mouse line; Lucie Jeannotte, Susan Parkhurst, and members of our laboratory for comments on the manuscript; Valeri Vasioukhin for comments and helpful discussions and the cadherin antibody; Brigid Hogan and Jean Charron for in situ probes; and Philip Corrin and Jason Frazier for skilled technical assistance and mice genotyping. J.A. and A.D. were recipients of postdoctoral fellowships from the Canadian Institutes for Health Research and Human Frontier Science Program, respectively. This work was supported by grants HD24875 and HD25326 from the National Institutes of Child Health and Human Development to P.S.

The publication costs of this article were defrayed in part by payment of page charges. This article must therefore be hereby marked "advertisement" in accordance with 18 USC section 1734 solely to indicate this fact.

References

Allard, S., Adin, P. Gouédard, L., di Clemente, N., Josso, N., Orgebin-Crist, M.-C., Picard, J.-Y., and Xavier, F. 2000. Molecular mechanisms of hormone-mediated Müllerian duct regression: Involvement of β-catenin. *Development* **127:** 3349–3360.

Aubin, J., Déry, U., Lemieux, M., Chailler, P., and Jeannotte, L. 2002. Stomach regional specification requires *Hoxa5*-driven mesenchymal–epithelial signaling. *Development* **129:** 4075–4087.

Balemans, W. and Van Hul, W. 2002. Extracellular regulation of BMP signaling in vertebrates: A cocktail of modulators. *Dev. Biol.* **250:** 231–250.

Behringer, R.R., Finegold, M.J., and Cate, R.L. 1994. Müllerian-inhibiting substance function during mammalian sexual development. *Cell* **79:** 415–425.

Berghella, L., De Angelis, L., Coletta, M., Berarducci, B., Sonnino, C., Salvatori, G., Anthonissen, C., Cooper, R., Butler-Browne, G.S., Mouly, V., et al. 1999. Reversible immortalization of human myogenic cells by site-specific excision of a retrovirally transferred oncogene. *Hum. Gene Therapy* **10:** 1607–1617.

Brembeck, F.H., Schreiber, F.S., Deramaudt, T.B., Craig, L., Rhoades, B., Swain, G., Grippo, P., Stoffers, D.A., Silberg, D.G., and Rutsgi, A.K. 2003. The mutant K-ras oncogene causes pancreatic periductal lymphcytic infiltration and gastric mucous neck cell hyperplasian in transgenic mice. *Cancer Res.* **63:** 2005–2009.

Calonge, M.J. and Massagué, J. 1999. Smad4/DPC4 silencing and hyperactive Ras jointly disrupt Transforming Growth Factor-β antiproliferative responses in colon cancer cells. *J. Biol. Chem.* **274:** 33637–33643.

Chang, H. and Matzuk, M. 2001. Smad5 is required for mouse primordial germ cell development. *Mech. Dev.* **104:** 61–67.

Chang, H., Huylebroeck, D., Verschueren, K., Guo, Q., Matzuk, M.M., and Zwijsen, A. 1999. Smad5 knockout mice die at mid-gestation due to multiple embryonic and extraembryonic defects. *Development* **128:** 1631–1642.

De Caestecker, M.P., Parks, W.T., Frank, C.J., Castagnino, P., Bottaro, D.P., Roberts, A.B., and Lechleider, R.J. 1998. Smad2 transduces common signals from receptor serine–threonine and tyrosine kinases. *Genes & Dev.* **12:** 1587–1592.

Derynck, R. and Zhang, Y.E. 2003. Smad-dependent and Smad-independent pathways in TGF-β family signaling. *Nature* **425:** 577–584.

Downs, K.M., Hellman, E.R., McHugh, J., Barrickman, K., and Inman, K.E. 2003. Investigation into a role for the primitive streak in development of the murine allantois. *Development* **131:** 37–55.

Foletta, V.C., Lim, M.A., Soosairajah, J., Kelly, A.P., Stanley, E.G., Shannon, M., He, W., Das, S., Massagué, J., and Bernard, O. 2003. Direct signaling by the BMP type II receptor via the cytoskeletal regulator LIMK1. *J. Cell Biol.* **162:** 1089–1098.

Fujiwara, T., Dunn, N.R., and Hogan, B.L.M. 2001. Bone morphogenetic protein 4 in the extraembryonic mesoderm is required for allantois development and the localization and survival of primordial germ cells in the mouse. *Proc. Natl. Acad. Sci.* **24:** 13739–13744.

Gordon, J.I. and Hermiston, M.L. 1994. Differentiation and self-renewal in the mouse gastrointestinal epithelium. *Curr. Opin. Cell Biol.* **6:** 795–803.

Grimm, O. and Gurdon, J.B. 2002. Nuclear exclusion of Smad2 is a mechanism leading to loss of competence. *Nat. Cell Biol.* **4:** 519–522.

Hayashi, K., Tobayashi, T., Umino, T., Goitsuka, R., Matsui, Y., and Kitamura, D. 2002. SMAD1 signaling is critical for initial commitment of germ cell lineage form mouse epiblast. *Mech. Dev.* **118:** 99–109.

Hoodless, P.A., Haerry, T., Abdollah, S., Stapleton, M., O'Connor, M.B., Attisano, L., and Wrana, J.L. 1996. MADR1, a MAD-related protein that functions in BMP2 signaling pathways. *Cell* **85:** 489–500.

Hu, M.C., Piscione, T.D., and Rosenblum, N.D. 2003. Elevated SMAD1/β-catenin molecular complexes and renal medullary cystic dysplasia in ALK3 transgenic mice. *Development* **130:** 2753–2766.

Huang, S., Flanders, K.C., and Roberts, A.B. 2000. Characterization of the mouse Smad1 gene and its expression pattern in adult mouse tissues. *Gene* **258:** 43–53.

Jamin, S.P., Arango, N.A., Mishina, Y., Hanks, M.C., and Behringer, R. 2000. Requirement of Bmpr1a for Mullerian duct regression during male sexual development. *Nat. Genet.* **32:** 408–410.

Kretzschmar, M., Doody, J., and Massagué, J. 1997a. Opposing BMP and EGF signalling pathways converge on the TGF-β family mediator Smad1. *Nature* **389:** 617–622.

Kretzschmar, M., Liu, F., Hata, A., Doody, J., and Massagué, J. 1997b. The TGF-β family mediator Smad1 is phosphorylated directly and activated functionally by the BMP receptor kinase. *Genes & Dev.* **11:** 984–995.

Kretzschmar, M., Doody, J., Timokhina, I., and Massagué, J. 1999. A mechanism of repression of TGF/Smad signaling by oncogenic Ras. *Genes & Dev.* **13:** 804–816.

Lawson, K.A., Dunn, N.R., Roelen, B.A.J., Zeinstra, L.M., Davis, A.M., Wright, C.V.E., Korving, J.P.W.F.M., and Hogan, B.L.M. 1999. *Bmp4* is required for the generation of primordial germ cells in the mouse embryo. *Genes & Dev.* **13:** 424–436.

Lechleider, R.J., Ryan, J.L., Garrett, L., Eng, C., Deng, C., Wynshaw-Boris, A., and Roberts, A.B. 2001. Targeted mutagenesis of Smad1 reveals an essential role in chorioallantoic fusion. *Dev. Biol.* **240:** 157–167.

Lehmann, K., Janda, E., Pierreux, C.E., Rytömaa, M., Schulze, A., McMahon, M., Hill, C.S., Beug, H., and Downward, J. 2000. Raf induces TGFβ production while blocking its apoptotic but not invasive responses: A mechanism leading to increased malignancy in epithelial cells. *Genes & Dev.* **14:** 2610–2622.

Li, Q., Karam, S.M., and Gordon, J.I. 1996. Diphtheria toxin-mediated ablation of parietal cells in the stomach of transgenic mice. *J. Biol. Chem.* **271:** 3671–3676.

Massagué, J. 2003. Integration of Smad and MAPK pathways: A link and a linker revisited. *Genes & Dev.* **17:** 2993–2997.

Massagué, J. and Wotton, J. 2000. Transcriptional control by the TGF-β/Smad signaling system. *EMBO J.* **19:** 1745–1754.

Mishina, Y., Rey, R., Finegold, M.J., Matzuk, M.M., Josso, N., Cate, R.L., and Behringer, R.R. 1996. Genetic analysis of the Mullerian-inhibiting substance signal transduction pathway in mammalian sexual differentiation. *Genes & Dev.* **10:** 2577–2587.

Narita, T., Saitoh, K. Kameda, T., Kuroiwa, A., Mizutani, M., Koike, C., Iba, H., and Yasugi, S. 2000. BMPs are necessary for stomach gland formation in the chicken embryo: A study using virally induced BMP-2 and Noggin expression. *Development* **127:** 981–988.

Okamura, D., Kumura, T., Nakano, T., and Matsui, Y. 2003. Cadherin-mediated cell interaction regulates germ cell determination in mice. *Development* **130:** 6423–6430.

Pellegrini, M., Grimaldi, P., Rossi, P., Geremia, R., and Dolci, S. 2003. Developmental expression of BMP4/ALK3/SMAD5 signaling pathway in the mouse testis: A potential role of BMP4 in spermatogonia differentiation. *J. Cell Sci.* **116:** 3363–3372.

Pera, E. Ikeda, A., Eivers, E., and De Robertis, E.M. 2003. Integration of IGF, FGF and anti-BMP signals via Smad1 phosphorylation in neural induction. *Genes & Dev.* **17:** 3023–

3028.
Qin, B.Y., Chacko, B.M., Lam, S.S., de Caestecker, M.P., Correia, J.J., and Lin, K. 2001. Structural basis of Smad1 activation by receptor kinase phosphorylation. *Mol. Cell* **8:** 1303–1312.
Roberts, D. 2000. Molecular mechanisms of development of the gastrointestinal tract. *Dev. Dynam.* **219:** 109–120.
Siegel, P.M. and Massagué, J. 2003. Cytostatic and apoptotic actions of TGF-β in homeostasis and cancer. *Nat. Rev. Cancer* **3:** 807–820.
Smith, D.M., Nielsen, C., Tabin, C.J., and Roberts, D. 2000. Roles of BMP signaling and Nkx2.5 in patterning at the chick midgut–foregut boundary. *Development* **127:** 3671–3681.
Tallquist, M.D. and Soriano, P. 2000. Epiblast restricted Cre expression in MORE mice: A tool to distinguish embryonic vs. extra-embryonic gene function. *Genesis* **26:** 113–115.
Tremblay, K.D., Dunn, N.R., and Robertson, E.J. 2001. Mouse embryos lacking Smad1 signals display defects in extra-embryonic tissues and germ cell formation. *Development* **128:** 3609–3621.
Wilkinson, D.G. and Nieto, M.A. 1993. Detection of messenger RNA by in situ hybridization to tissue sections and whole mounts. *Meth. Enzymol.* **225:** 361–373.
Ying, Y. and Zhao, G.-Q. 2001. Cooperation of endoderm-derived BMP2 and extraembryonic ectoderm-derived BMP4 in primordial germ cell generation in the mouse. *Dev. Biol.* **232:** 484–492.
Ying, Y., Liu, X.-M., Marble, A.M., Lawson, K.A., and Zhao, G.-Q. 2000. Requirement of *Bmp8b* for the generation of primordial germ cells in the mouse. *Mol. Endocrinol.* **14:** 1053–1063.
Yue, J., Frey, R.S., and Mulder, K.M. 1999. Cross-talk between Smad1 and Ras/MEK signaling pathways for TGFβ. *Oncogene* **58:** 4752–4757.
Zakin, L. and De Robertis, E.M. 2004. Inactivation of mouse *Twisted gastrulation* reveals its role in promoting Bmp4 activity during forebrain development. *Development* **131:** 413–424.
Zhu, C.-H. and Xie, T. 2003. Clonal expansion of ovarian germline stem cells during niche formation in *Drosophila*. *Development* **130:** 2579–2588.